A&A 463, 265–274 (2007)
DOI: 10.1051/0004-6361:20052807

Astronomy & Astrophysics

Chemical compositions and plasma parameters of planetary nebulae with Wolf-Rayet and wels type central stars⋆,⋆⋆,⋆⋆⋆

P. Girard[1,2], J. Köppen[2,3,4], and A. Acker[2]

[1] Observatoire Aquitain des Sciences de l'Univers, L3AB, 2 rue de l'Observatoire, BP 89, 33270 Floirac, France
e-mail: girard@obs.u-bordeaux1.fr
[2] Observatoire Astronomique de Strasbourg, 11 rue de l'Université, 67000 Strasbourg, France
[3] Institut für Theoretische Physik und Astrophysik, Universität Kiel, 24098 Kiel, Germany
[4] International Space University, Parc d'Innovation, 67400 Illkirch, France

Received 2 February 2005 / Accepted 20 October 2006

ABSTRACT

Aims. Chemical compositions and other properties of planetary nebulae around central stars of spectral types [WC], [WO], and *wels* are compared with those of "normal" central stars, in order to clarify the evolutionary status of each type and their interrelation.
Methods. We use plasma diagnostics to derive from optical spectra the plasma parameters and chemical compositions of 48 planetary nebulae. We also reanalyze the published spectra of a sample of 167 non-WR PN. The results as well as the observational data are compared in detail with those from other studies of the objects in common.
Results. We confirm that [WC], [WO] and *wels* nebulae are very similar to those "normal" PN: the relation between [N II] and [O III] electron temperatures, abundances of He, N, O, Ne, S and Ar, and the number of ionizing photons show no significant differences. However, some differences are observed in their infrared (IRAS) properties. *wels* nebulae appear bluer than [WR] PN. The central star's spectral type is clearly correlated with electron density, temperature and excitation class of the nebula, [WC] nebulae tend to be smaller than the other types. All this corroborates the view of an evolutionary sequence from cool [WC 11] central stars inside dense, low excitation nebulae towards hot [WO 1] stars with low density, high excitation nebulae. The *wels* PN, however, appear to be a separate class of objects, not linked to WRPN by evolution: nebular excitation, electron temperature and density, and the number of ionizing photons all cover the whole range found in the other types. Their lower mean N/O ratio and slightlylower He/H suggest progenitor stars less massive than for the other PN types. Furthermore, the differences between results of different works are dominated by the differences in observational data rather than differences in the analysis methods.

Key words. planetary nebulae: general – stars: abundances – stars: evolution – stars: Wolf-Rayet – stars: AGB and post-AGB

1. Introduction

Planetary nebulae (PN) are the highly visible transitionary phase in the life of intermediate mass stars on their evolution from the asymptotic giant branch to their final destination, the white dwarfs. Among the 1300 objects known in our Milky Way (Acker et al. 1992, 1996b), there are about 6% whose central stars show broad emission lines, characteristic of the [WR] spectral type, and most likely produced by a massive continuous mass loss from the central star. Whether these objects form a group or an evolutionary phase or evolutionary sequence distinctly different from the other, "normal" PN, is still not fully understood.

That PN with [WR] central stars do not seem to have properties which differ very much from normal, non-WR objects was shown by Górny & Stasińska (1995) who found that bipolar nebulae constitute about 20 % of the total in both WR and non-WR objects. Also, the distribution of He/H, N/O and C/O abundance ratios are the same in either group. Both aspects indicate that the WR phenomenon does not preferentially occur in more massive central stars, hence more massive progenitor stars. Acker et al. (1996a), Górny & Tylenda (2000) and Peña et al. (2001) showed that the majority of [WR] PN seems to form an evolutionary sequence from late-type [WC] inside high-density nebulae to early-type [WO] with low-density nebulae.

In their recent quantitative classification of central stars, Acker & Neiner (2003) distinguish two sequences from the late-type [WC] to the early-type [WO]: the spectra of hot [WO 1...4] types are dominated by the highly ionised oxygen lines, while those of the cooler [WC 4...11] types are marked by carbon lines. There seems to be an evolutionary sequence from [WC 11] to [WO 1]. The *wels* (weak emission line stars) objects differ from other central stars (Tylenda, Acker & Stenholm 1993) and are not part in this classification scheme.

More recently, Górny et al. (2004) found that the proportion of WRPN in the Galactic bulge is about 15%, significantly larger than in the disk (about 6%). Among the bulge WRPN about 47% are of type later than [WC 9]. In the disk this fraction amounts to only 17%. However, this finding is strongly sensitive to observational selection effects. They confirm the strong trend for the density to decrease towards early-type [WC]. Oxygen abundances in bulge WRPN are found to be the same as in the

⋆ Based on observations obtained at the European Southern Observatory (ESO), La Silla, Chile.
⋆⋆ Table 3 and Appendices are only available in electronic form at http://www.aanda.org
⋆⋆⋆ Table with fluxes and intensities is only available in electronic form at the CDS via anonymous ftp to cdsarc.u-strasbg.fr(130.79.128.5) or via http://cdsweb.u-strasbg.fr/cgi-bin/qcat?J/A+A/463/265

bulge non-WR, and the N/O distributions of PN in disk, bulge and of [WR] type are similar.

Another age indicator is the dust temperature derived from near and mid infrared data, indicating an evolutionary sequence from carbon AGB stars to [WC] PNe (Acker et al. 1996a). Gòrny et al. (2001) found that a sizeable fraction of WRPN seems to contain hot dust (1000–2000 K), probably in the winds of the central stars. The mean dust temperature decreases towards late-type [WC], in line with an evolutionary sequence from [WC11] to [WC2] ([WO2]).

The present paper presents the study of a homogeneous sample of nebulae around nuclei with emission lines, using the high S/N spectra which had been used to study the [WR] central stars by Acker & Neiner (2003). These objects constitute a sample similar to that of Peña et al. (2001), and it seems interesting to confirm (or not) the conclusions of these authors as well as those by Górny et al. (2004).

After presenting the observational material in Sect. 2 and describing the analysis of the spectra in Sect. 3, we study the chemical compositions of the various types of nebulae in Sect. 4. We also compare the different groups with respect to other global relations in Sect. 5, investigate the relation between central stars and the nebulae (Sect. 6), and analyse the infrared properties (Sect. 7). In Appendices A and B we study the influences on the abundances due to differences in observational data and analysis methods.

2. Observational material

90 spectra of PN around central stars with emission lines were obtained in March 1994, July 1994, and July 1995 with the Boller & Chivens spectrograph and the CCD detector on the 1.52 m telescope at ESO, Chile. The wavelength range is from 3700 Å to 7500 Å, with a spectral resolution of 1500 (more details can be found in Acker & Neiner 2003). Exposure times of 40 min and 5 min were employed, giving signal to noise ratios of better than 30 for most objects. For the analyses, the 48 objects with the best spectra were selected.

The measured line fluxes and dereddened intensities from the spectra of 48 planetary nebulae with emission line-stars used in this work are available in electronic form at the CDS. The quality of the data and their reduction can be assessed by looking at the line ratio of the [O III] 5007 and 4959 Å doublet which is independent of physical conditions in the nebula. Figure 1 shows that in all objects values very close to 3.0 are found, but slightly above the theoretical value from Mendoza (1983), as expected (cf. Acker et al. 1989). Only a few objects with faint spectra exhibit somewhat larger deviations.

Another check is provided by the intensity ratios of the dereddened He I lines at 5876, 4471, and 6678 Å which are not very sensitive to nebular conditions. All 33 objects which contain the three lines are found within 20 percent of the theoretical values (Fig. 2).

Since a number of the objects have been observed by other authors, we compared our data in detail with previous measurements. The He II 4686 Å line covers a large range in values among the objects. As shown by Fig. 3, our (dereddened) intensities agree very well with those obtained by other authors. In particular, the agreement with the most recent study of Peña et al. (2001, PSM01) is better than 0.1 dex. As one should expect, the scatter increases towards fainter intensities.

A comparison of the He I 5876 Å lines (Fig. 4) shows a good agreement with other studies. However, one notes a

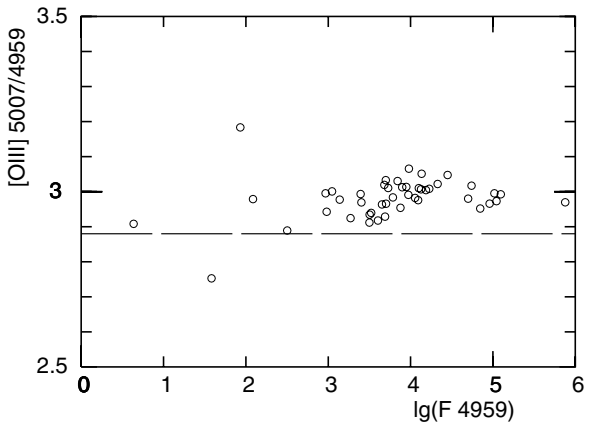

Fig. 1. The intensity ratio of the [O III] 5007 and 4959 Å lines as a function of the flux (arbitrary units) in the 4959 Å line. The horizontal line indicates the value expected from the atomic data compiled by Mendoza (1983).

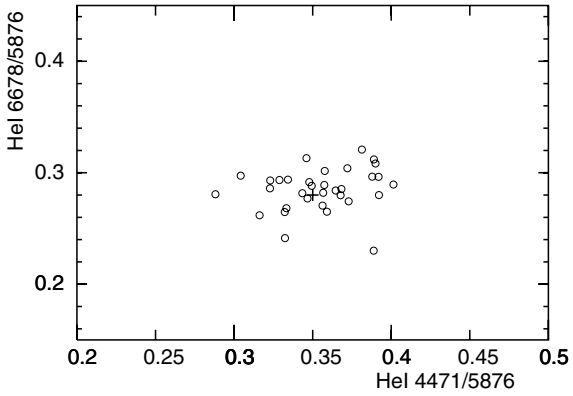

Fig. 2. The intensity ratios of the HeI 5876, 4471, and 6678 Å lines. The plus sign marks the low density value for $T_e = 10^4$ K.

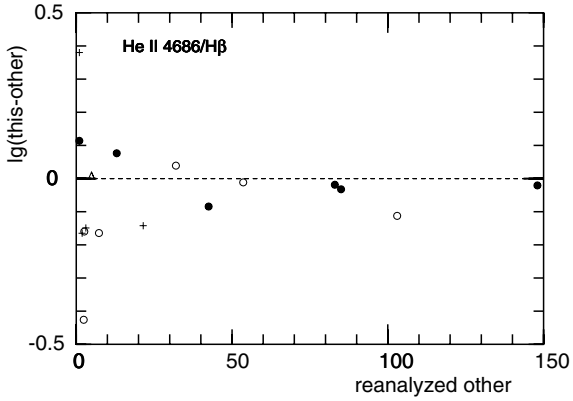

Fig. 3. The relative difference in intensity of the He II 4686Åline of our measurements compared to those of other works: Aller & Keyes (1987, AK87, +), Kingsburgh & Barlow (1994, KB94, ○), Cuisinier et al. (1996, CAK96, △), and Peña et al. (2001, PSM01, •)

trend, in that our intensities tend to be larger than those of Kingsburgh & Barlow (1994, KB94), but smaller than those by PSM01 which is especially obvious for larger intensities. Objects with large deviations are the [WO]s PNG 002.4 + 05.8, PNG 003.1 + 02.9, PNG 017.9 − 04.8, PNG 278.1 − 05.9, the [WC]s PNG 006.8 + 04.1, PNG 027.6 + 04.2, PNG 048.7 + 01.9,

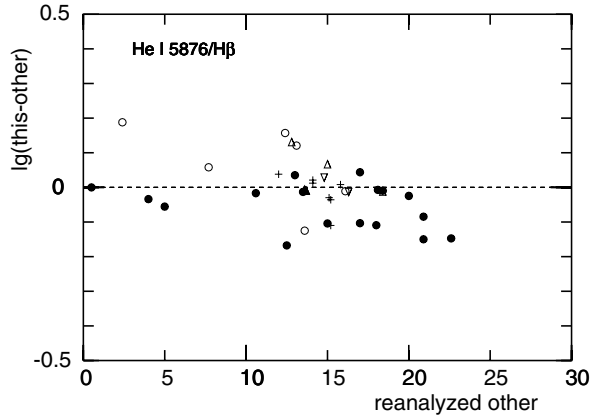

Fig. 4. The intensity of HeI 5876 Å line compared to the value obtained by other works. Symbols are as in Fig. 3 plus Cuisinier et al. (2000, CMAKS00, ▽).

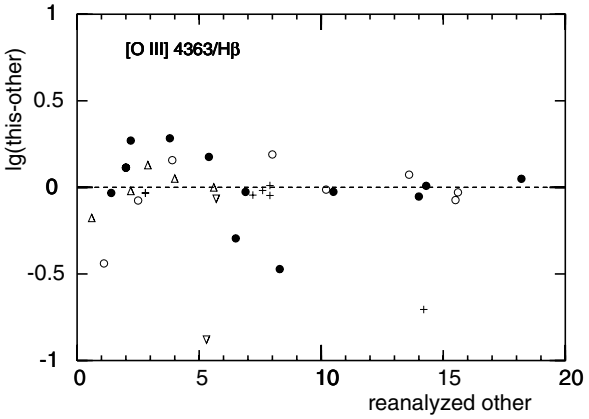

Fig. 5. The measured intensity of the [O III] 4363 Å line compared to the values obtained by the other works. Symbols are as in Fig. 4.

and the *wels* PNG 010.8 − 01.8. Since [WO] nebulae exhibit no stellar He I lines (cf. Acker & Neiner 2003), it is unlikely that our measurements are affected by confusion with the stellar spectrum. Furthermore, inspection of the other He I lines (4471, 6678, 7065, and 5015 Å) shows that these line ratios are in good agreement with the intensity of the 5876 line.

The [O III] 4363 Å diagnostic line is of similar strength as the He I 5876 Å line. As shown in Fig. 5, our measurements are in good to fair agreement with the intensities obtained by the other studies. For intensities below 10 percent of Hβ the deviations with PSM01 are as large as a factor of two, in either direction.

A similar finding is obtained for the [S II] 6717/31 Å doublet.

As a consequence of the difference in He I line intensities, our helium abundances differ slightly from the results of PSM01. This is addressed in more detail in Appendix B. However, it does not affect the findings of this paper with respect to the evolutionary status of the [WR] PN.

2.1. A sample of "normal" PNe

To compare the sample of [WR] nebulae with "normal" PN, we selected the objects from the following works: Aller & Czyzak (1983, hereafter AC83), Aller & Keyes (1987, AK87), Cuisinier et al. (1996, CAK96), Cuisinier et al. (2000, CMAKS00) and Kingsburgh & Barlow (1994, KB94). Although the image tube data from AC83 and AK87 might be considered less reliable than present CCD data, such a suspicion is not too evident in individual comparisons. Moreover, these works constitute a large sample of the brighter PN, together with KB94. We include CAK96 who focussed on objects high above the Galactic plane as well as the sample of Bulge nebulae by CMAKS00. The inclusion of these samples does not constitute a major bias, since in our sample of [WR] objects there also is no selection against nebulae outside the disk.

To avoid possible influences by the different analysis methods employed by the other authors, we re-analyzed all the other spectra by our method using the same criteria. This includes using only the optical lines in the spectra of KB94. All together, this sample provides 167 objects with spectra of comparable quality which had been obtained for determinations of chemical compositions.

2.2. Comparison with other works

There are 3 nebulae in common with AC83, 7 with AK87, 8 with KB94, 6 with CAK96, 2 with CMAKS00, and in particular 17 with PSM01. This offers an opportunity to clarify to what extent the results from different studies are subject to differences in the measured line fluxes or to the adopted abundance determination methods. In Appendix A we compare the results obtained from reanalysis of the data by HOPPLA with the original values. The differences in the observational data are addressed in Appendix B.

3. Plasma analysis of the nebular spectra

Extinction constants, electron temperatures and densities, and elemental abundances are determined with the computer programme HOPPLA (see Acker et al. 1991, and Köppen et al. 1991). The spectra are interpreted by the technique of plasma diagnostics, viz. assuming that all lines are produced in an isothermal gas at uniform density and ionization level. In the first step, the reddening correction, derivation of electron temperature and density, as well as the optical depth of the He I 3888 Å line (for self-absorption in the He I lines) are performed. These steps are repeated several times, until the values converge.

The excitation class (EC), absolute Hβ fluxes seen through the spectrograph aperture, extinction constants c, electron temperatures and densities for all selected 48 PN are compiled in Table 2. The column "Q" gives an indication of the overall quality of the analysis. "A" means that all diagnostic lines are present, "B" that the density could not be reliably determined, and "C" that the electron temperature could not be derived.

The extinction measure c is obtained from the decrement of all the observed Balmer lines relative to the one computed from Brocklehurst (1972) for case B. To find the optimum value, the error from each line is weighted with the square of the observed line flux. This weighting had been chosen to be able to deal also with rather noisy spectra; for the present data this suppresses the noise in the blue region of the spectrum, by giving a strong weight to the Hα/Hβ ratio. In Fig. 6 we compare our values of the extinctions against the results found by other authors. For most of the objects we obtain good agreement; yet for several nebulae rather discrepant values have been reported, most probably due to the difficulty to separate the nebular from the stellar emission lines. Notable exceptions are collected in Table 1.

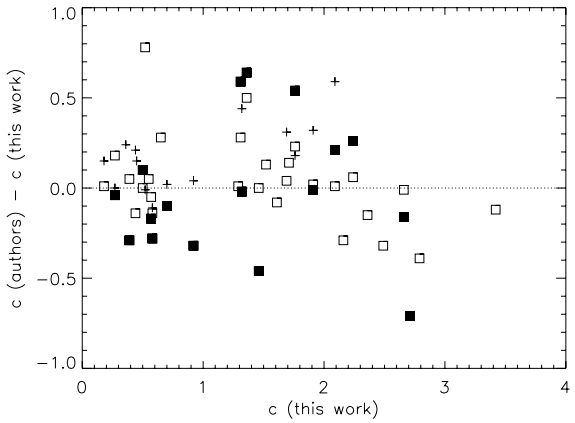

Fig. 6. The extinctions found in this work compared to other works for the same nebulae. Open squares refer to Acker & Neiner (2003) (from Crowther et al. 1998 and Tylenda et al. 1992), filled squares to PSM01, and plus-signs to AC83, Aller & Keyes (1980, 1987), Aller et al. (1981, 1986), Barker (1978), KB94, and Shaw & Kaler (1989)

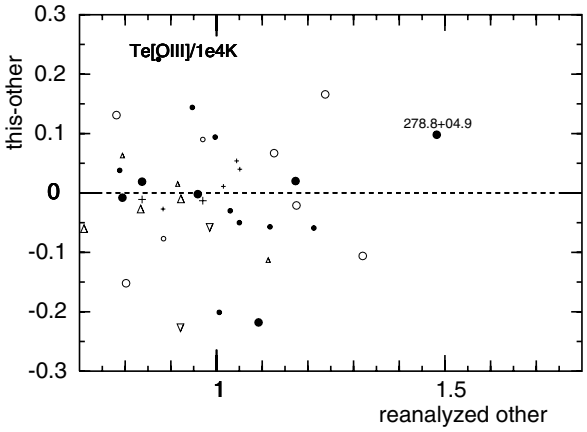

Fig. 7. Comparison of the [O III] electron temperatures derived in this work and determined by other authors for the same objects; symbols are the same as in Fig. 3. Smaller symbols indicate that in the other work the values were marked as uncertain.

Table 1. Nebulae whose extinctions found in this work and in the literature show strong differences. Other works are indicated by their abbreviations (e.g. KB94 for Kingsburgh & Barlow 1994) used in the References

PN G	This work	Other works	
002.2 – 09.4	0.39	0.44 TASK92,	0.1 PSM01
004.9 + 04.9	1.46	1.46 TASK92,	1.0 PSM01
009.4 – 05.0	0.92	0.96 AK87,	0.6 PSM01
017.9 – 04.8	0.52	0.51 SK89,	1.30 TASK92
061.4 – 09.5	0.00	0.09 AC83,	0.27 KB94,
		0.45 CMB98,	0.23 PSM01
292.4 + 04.1	0.68	0.38 TASK92,	2.7: KB94
300.7 – 02.0	2.49	2.17 TASK92	
331.3 + 16.8	0.36	0.64 KB94	
358.3 – 21.6	0.18	0.33 AKF86	

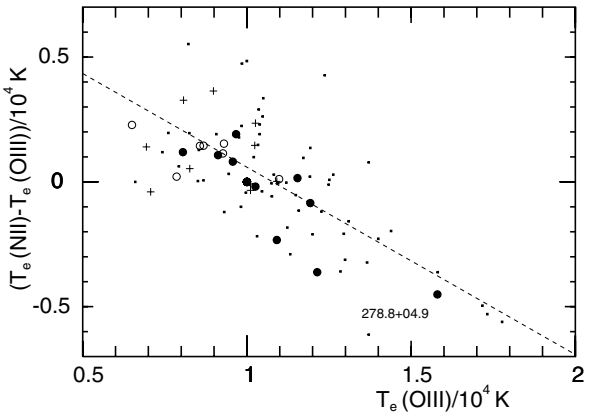

Fig. 8. Relation between difference of electron temperatures from [N II] and [O III] line ratios with the [O III] electron temperatures for PN with central stars of types [WO] (filled circles), [WC] (open circles), *wels* (plus-signs), and any other (small dots). The dotted line indicates the regression line obtained from the "normal" PN only.

Electron temperatures T_e are derived from line intensity ratios of [O III] (4959 Å + 5007 Å)/4363 Å and [N II] (6548 Å + 6584 Å)/5755 Å. We note that the high [N II] temperature in PNG 337.4 + 01.6 is the consequence of its density to be close to the high density limit of the [S II] lines. Figure 7 shows the comparison of our values of the [O III] temperature for the objects common with other authors. There is an overall good agreement and no obvious systematic offset. In particular, we confirm the rather high temperature in PNG 278.8+04.9 as found by PSM01.

Figure 8 shows the relation between the difference between [N II] and [O III] temperatures with [O III] temperatures for the [WR] and *wels* PN in comparison with the data for the non-WR PN. In nebulae of low electron temperature, the [N II] temperature exceeds the one in [O III], but in nebulae of high electron temperature the [N II] temperature is lower. From 74 "normal" PN one obtains a very tight correlation, with a coefficient of −0.74:

$$(T_e([\mathrm{N\,II}]) - T_e([\mathrm{O\,III}]) = (8090 \pm 923) - (0.750 \pm 0.080) \times T_e([\mathrm{O\,III}]) \quad (1)$$

which is displayed in Fig. 8. Taking all [WO] and [WC] PN together, one obtains from 24 objects a similarly tight correlation (coefficient −0.86):

$$(T_e([\mathrm{N\,II}]) - T_e([\mathrm{O\,III}]) = (7780 \pm 995) - (0.770 \pm 0.97) \times T_e([\mathrm{O\,III}]) \quad (2)$$

which is nearly identical. Taking the only 12 [WC], the slope is flatter −0.509 ± 0.144 and a correlation coefficient of −0.74 is found; from 11 [WO] PN one gets a slope of −0.854 ± 0.174 and a coefficient of −0.85. Thus the [WR] objects follow rather closely the relation seen among the "normal" PN. Only a larger sample would permit to judge whether the difference between [WO] and [WC] is really significant. As is already apparent from their scattered positions in Fig. 8, the 10 *wels* PN do not yield a significant correlation. The strong tendency for the "normal" PN objects to have larger [N II] temperatures has already been found by Górny et al. (2004) but not for the [WR] objects. From their Fig. 2 one also notes a tendency that in the hotter nebulae [N II] temperatures are lower than the ones from [O III].

The lower electron temperatures in the [WR] objects are also evident in the histogram (Fig. 9). The average temperature is 10 440 ± 390 K from 28 [WR] objects, somewhat lower than

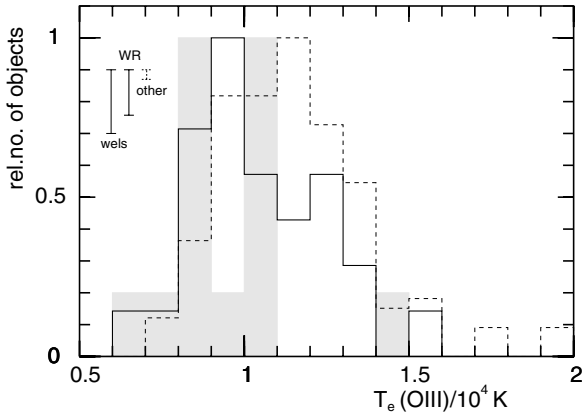

Fig. 9. Histograms of the [O III] electron temperature for the [WR] objects (full line), the *wels* PN (shaded area) and the objects with "normal" central stars (dashed). The vertical error bars indicate the contribution by a single object.

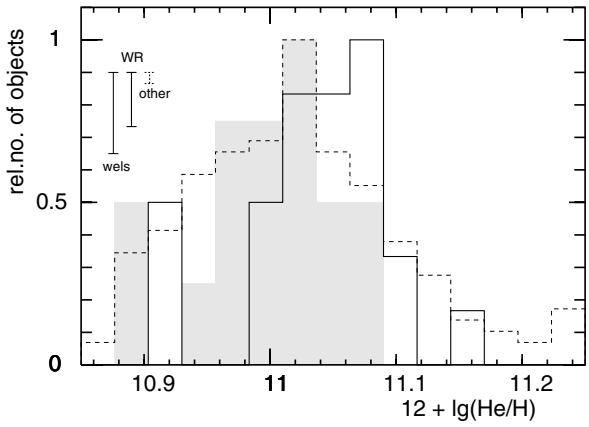

Fig. 10. Distribution of helium abundances among [WR] PN (full line), *wels* objects (shaded area), and nebulae around "normal" central stars (dashed line). The vertical error bars indicate the contribution by a single object.

11 680 ± 200 K from the 164 "normal" PN; the dispersions are also quite similar: 2070 ± 280 K and 2620 ± 140 K, respectively. Much more different are the *wels* nebulae: with a single exception of PNG 331.3 + 16.8, the 14 objects have [O III] temperatures in the narrow range between about 8000 and 11 000 K, as is also apparent in Fig. 8. The mean is 9390±460 and the dispersion 1740 ± 330 K, which includes the singular PNG 331.3 + 16.8.

Inspection of the temperatures and excitation classes shows a mild tendency for both [N II] and [O III] temperatures to increase with increasing excitation class, but no significant difference could be found in the behaviour of [WR] and normal PN. PNG 278.8 + 04.9 remains exceptional in having one of the highest [O III] temperatures found among any PN; the other objects seen in Fig. 8 in its vicinity are PNG 086.5 − 08.8 (data from AC83), PNG 245.4 + 01.6, PNG 261.6 + 03.0, and PNG 275.8 − 02.9 (from KB94).

Electron densities n_e are determined from the intensity ratios of the doublet [S II] 6717/6731 Å. If the [S II] lines cannot be measured, we use the [Cl III] 5517/5537 Å ratio (indicated by "C" in Table 2). In several nebulae the [S II] line ratio is close to the high-density limit. PNe whose density exceeds 20 000 cm^{-3} are marked by a "H" in Table 2 and this adopted value is used in further analysis.

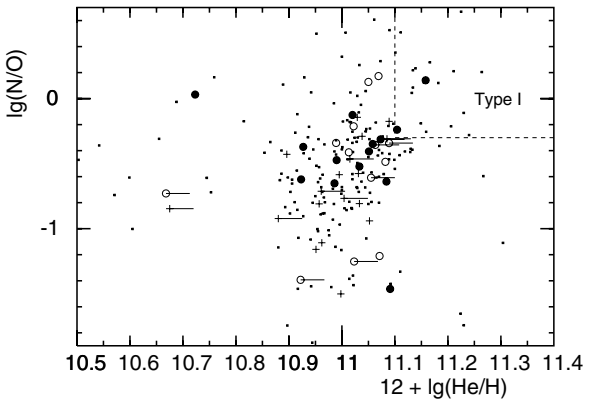

Fig. 11. Relation between helium abundances and N/O abundance ratios for WR, *wels* and "normal" PN. The symbols are as in Fig. 8. Short bars indicate a lower limit to the He abundance in WRPN of excitation class below 5.

4. Chemical compositions of the nebulae

With the electronic temperatures and densities obtained from the analysis of line ratios described above, the emissivities of all lines can be computed and thus from the observed dereddened intensities the ionic abundances relative to H^+ are deduced. Whenever both [N II] and [O III] electron temperatures are available, we use the [N II] temperature for the low ionization species (N^+, O^+, S^+, S^{++}) and the [O III] temperature for the higher species (O^{++}, Ne^{++}, Ar^{++},Ar^{3+}). To correct for unseen stages of ionization, the usual empirical correction factors (ICF) are applied (see Aller 1984). Table 3 (on-line version), presents the derived abundances of the 48 nebulae. All abundances are expressed in the usual logarithmic form of 12 + lg(n(X)/n(H)).

For helium, the abundances of He^+ and He^{++} are derived from the He I and He II recombination lines. The emissivities of the He I lines are corrected for self-absorption and collisional excitation. In low excitation nebulae there could be present an appreciable amount of unobservable neutral helium. Therefore the He abundances in low excitation nebulae (EC 4 and less) are only lower limits and are marked with a colon in Table 3 (on-line version). For the sulphur ICF, we use the recipe of Samland et al. (1992), while for chlorine we apply a simple formula that gave a reasonable approximation to results from photoionization models:

$$\frac{\mathrm{Cl}}{\mathrm{H}} \approx \frac{\mathrm{Cl}^{++}}{\mathrm{H}^{+}} \left(\frac{\mathrm{He}}{\mathrm{He}^{+}}\right)^{2}.$$

4.1. Elements synthesized in progenitor stars

Helium and nitrogen are elements that are produced in more massive progenitor stars of PN. Hence abundances of these elements is expected to be an indicator of the mass of the progenitor star. Comparing the histogram of helium abundances (Fig. 10), we find no evidence for any significant difference between the different types. Using only data without colon and quality code $Q = A$ analyses from 11 [WR] PN, 14 *wels*, and 87 "normal" PN, we obtain respective average values of 11.05±0.02, 10.97±0.03, and 11.02 ± 0.01, which places the [WR] PN above the solar value and the normal PN, but the *wels* have lower helium abundances. The dispersions are 0.05 ± 0.01, 0.10 ± 0.02, and 0.10 ± 0.01, respectively.

Table 2. Plasma parameters of the planetary nebulae of this sample. The spectral types are from Acker & Neiner (2003). Given are: overall quality of the analysis (see the text), excitation classes EC following Aller's (1956) system, Hβ fluxes in erg s^{-1} cm^{-2}, extinction constant c, electron temperatures from the [O III] and [N II] line ratios in 10^4 K, electron density from the [S II] line ratio in units of 1000 cm^{-3}. Values marked with 'A' are default values assumed in absence of the line ratio; densities marked with "H" are lower limits because of the saturation of the [S II] ratio for high densities, densities marked with 'C' are from the [Cl III] lines.

PN G	common name	Spec.Type	Q	EC	lg(F(Hβ))	c	T(OIII)	T(NII)	n(SII)
000.4 – 01.9	M 2-20	WC5-6	A	4	−12.80	1.71	—	0.79	5.40
002.2 – 09.4	Cn 1-5	WO4pe	A	5	−11.75	0.42	0.87	—	4.82
002.4 + 05.8	NGC 6369	WO3	A	5	−13.50	1.91	0.80	0.92	1.74
003.1 + 02.9	Hb 4	WO3	A	6	−12.50	1.76	0.96	1.04	6.71
004.8 – 22.7	He 2-436	WC4	C	5	−12.39	0.55	1.00A	1.00A	12.92 C
004.9 + 04.9	M 1-25	WC4	A	4	−12.24	1.46	0.79	0.81	8.00
006.0 – 03.6	M 2-31	WC4	A	5	−12.50	1.29	0.93	1.08	5.31
006.4 + 02.0	M 1-31	wels	A	5	−12.73	2.00	—	0.99	11.70
006.8 + 04.1	M 3-15	WC4	A	5	−12.89	2.08	1.10	1.11	5.56
009.4 – 05.0	NGC 6629	wels	A	5	−12.16	0.92	0.86	—	2.13
010.8 – 01.8	NGC 6578	wels	A	5	−12.49	1.35	0.83	0.88	7.46
011.7 – 00.6	NGC 6567	wels	A	5	−11.47	0.70	1.09	1.09	10.46
011.9 + 04.2	M 1-32	WO4pe	A	4	−12.53	1.30	1.09	0.86	9.25
012.2 + 04.9	PM 1-188	WC10	C	<2	−14.53	1.36	1.00A	1.00A	2.29
016.4 – 01.9	M 1-46	wels	A	<2	−12.33	1.07	—	0.69	2.83
017.9 – 04.8	M 3-30	WO1	C	7	−14.07	0.52	1.00A	1.00A	3.40
019.4 – 05.3	M 1-61	wels	A	5	−11.74	1.71	0.93	—	16.41
019.7 – 04.5	M 1-60	WC4	A	5	−12.67	1.52	0.86	1.00	6.93
020.9 – 01.1	M 1-51	WO4pe	A	5	−13.92	3.37	—	0.88	7.73
027.6 + 04.2	M 2-43	WC7-8	C	4	−12.79	2.67	1.00A	1.00A	11.00 C
029.2 – 05.9	NGC 6751	WO4	A	5	−13.06	0.50	1.06	—	2.27
034.6 + 11.8	NGC 6572	wels	A	5	−10.73	0.30	1.02	1.17	17.41
038.2 + 12.0	Cn 3-1	wels	A	<2	−11.33	0.44	—	0.75	6.90
048.7 + 01.9	He 2-429	WC4	A	4	−13.36	2.21	—	0.84	7.16
055.5 – 00.5	M 1-71	wels	A	5	−12.52	2.18	0.90	1.26	12.39
057.2 – 08.9	NGC 6879	wels	A	5	−11.70	0.42	1.03	1.26	4.16
061.4 – 09.5	NGC 6905	WO2	B	7	−12.84	0.00 A	1.15	1.17	0.53
068.3 – 02.7	He 2-459	WC9	C	<2	−13.38	2.65	1.00A	1.00A	16.17
253.9 + 05.7	M 3-6	wels	A	5	−12.05	0.49	0.81	1.13	5.21
258.1 – 00.3	He 2-9	wels	A	4	−12.71	2.22	1.01	0.98	10.85
274.6 + 02.1	He 2-35	wels	A	5	−12.29	0.80	0.87	—	1.97 C
278.1 – 05.9	NGC 2867	WO2	A	7	−11.57	0.58	1.19	1.11	2.81
278.8 + 04.9	PB 6	WO1	A	7	−13.38	0.57	1.58	1.13	2.89
285.4 + 01.5	Pe 1-1	WO4	A	5	−12.72	2.16	0.97	1.16	18.31
291.3 – 26.2	Vo 1	WC10	C	<2	−14.15	2.19	1.00A	1.00A	5.00 C
292.4 + 04.1	PB 8	WC5-6	A	6	−12.01	0.67	0.65	0.88	3.99
300.7 – 02.0	He 2-86	WC4	A	5	−12.62	2.49	0.87	1.01	11.90
307.2 – 03.4	NGC 5189	WO1	A	5	−13.33	0.44	1.21	0.85	0.48
327.1 – 02.2	He 2-142	WC9	B	<2	−12.34	2.11	—	0.75	20.00 H
331.3 + 16.8	NGC 5873	wels	A	7	−11.56	0.37	1.40	—	5.19
336.2 – 06.9	PC 14	WO4	A	5	−12.16	0.65	0.91	1.02	3.05
337.4 + 01.6	Pe 1-7	WC9	B	<2	−12.69	2.79	—	1.64	20.00 H
351.1 + 04.8	M 1-19	wels	A	4	−12.27	1.24	0.69	0.83	5.49
355.2 – 02.5	H 1-29	WC4	A	5	−12.81	1.61	0.93	1.04	7.30
355.9 – 04.2	M 1-30	wels	A	3	−12.24	1.01	0.71	0.67	4.93
356.7 – 04.8	H 1-41	wels	A	7	−12.67	0.65	1.01	1.00	1.17
357.1 + 03.6	M 3-7	wels	A	4	−12.80	1.83	—	0.78	4.67
358.3 – 21.6	IC 1297	WO3	A	7	−11.62	0.18	1.03	1.01	2.80

Likewise, the relation between helium abundance and the N/O abundance ratio exhibits no clear difference between the two types of nebulae. Neither is obvious any difference between objects with [WO], [WC], or *wels* central stars, as depicted in Fig. 11. Two objects fullfill the criterion of Peimbert & Torres-Peimbert (1983) for Type I nebulae: the [WO] types PNG 002.2 – 09.4 and PNG 278.8 + 04.9, and with the *wels* PNG 006.4 + 02.0 doing nearly so.

The average helium abundances for all types, presented in Table 4, are solar without any significant differences. The nitrogen abundance in [WC] and [WO] is somewhat enhanced with respect to the Sun, but *wels* and "normal" PN have solar values. The N/O abundance ratio found in both [WC] and [WO] type nebulae is about thrice solar, but in "normal" nebulae it is not more than twice solar. The *wels* objects have nearly a solar ratio. One also notes that the helium abundance is somewhat lower, by about twice the standard error. It thus is tempting to identify *wels* nebulae as coming from less massive progenitor stars than the other types of PN.

4.2. The other elements

Oxygen, neon, sulphur, and argon are synthesized in massive stars, and their abundances are not altered by the nucleosynthesis in the PN progenitor stars. The average oxygen abundances, presented in Table 4, among [WC] and [WO] PN are slightly above the values found in *wels* and "normal" PN, all of which are significantly lower (about 0.3 dex) than the solar system abundance. Neon is close to solar values in all types. Sulphur is about 0.3 dex higher in [WO] and [WC] than in *wels* and "normal" PN. In all PN sulphur appears to be lower than the solar value; however, one has to keep in mind that the empirical ICF for sulphur is less accurate than for nitrogen or neon. Thus we do not want to exclude a systematic tendency for underestimating the sulphur abundances. Within the error bars, argon is also solar in all types

Table 4. Average abundances for the PN of each type, along with the dispersion. Only values without a colon in Table 3 from class "A" analyses are taken into account; numbers of objects used are given in parenthesis. The values for the non-WR sample come from our reanalysis of the published data. The solar system abundances are from Anders & Grevesse (1989).

Element	[WC]	[WO]	*wels*	non-WR	solar
He	11.06 ± 0.03 (3)	11.06 ± 0.06 (6)	10.97 ± 0.10 (14)	11.02 ± 0.10 (87)	10.99
N	8.43 ± 0.28 (9)	8.37 ± 0.23 (12)	7.94 ± 0.38 (18)	8.13 ± 0.55 (144)	8.05
O	8.70 ± 0.13 (9)	8.72 ± 0.14 (12)	8.64 ± 0.15 (18)	8.57 ± 0.26 (155)	8.93
Ne	7.93 ± 0.24 (8)	8.10 ± 0.25 (12)	7.94 ± 0.16 (15)	7.92 ± 0.30 (88)	8.09
S	7.05 ± 0.20 (9)	7.06 ± 0.25 (12)	6.79 ± 0.25 (17)	6.78 ± 0.30 (109)	7.21
Ar	6.58 ± 0.17 (7)	6.40 ± 0.25 (9)	6.34 ± 0.32 (12)	6.22 ± 0.28 (80)	6.56
N/O	−0.27 ± 0.25 (9)	−0.35 ± 0.25 (12)	−0.70 ± 0.35 (18)	−0.44 ± 0.48 (143)	−0.88

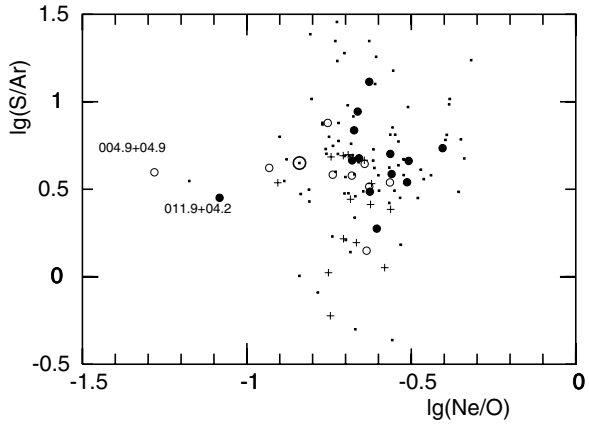

Fig. 12. Relation between the abundance ratios Ne/O and S/Ar. The symbols are as in Fig. 8. The solar symbol indicates solar values (lg(Ne/O) = −0.84 and lg(S/Ar) = 0.65).

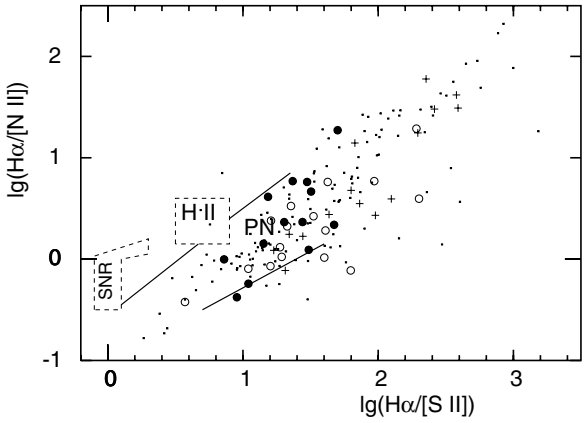

Fig. 13. The intensity ratios Hα/[N II] and Hα/[S II] of our objects, in relation to the regions identified by Cantó (1981). The symbols are as in Fig. 8.

of nebulae. Therefore, the chemical compositions of planetary nebulae with central stars of types [WC], [WO], and *wels* appear to differ somewhat from those of nebulae with "normal" central stars, with nearly solar system values.

The abundance ratios Ne/O and S/Ar, shown in Fig. 12, of either type of PN are rather close to the ratios found in the Sun. As already seen from Table 4, all PN cluster around the solar system value for S/Ar ratio, but at higher Ne/O ratio. The distributions of the [WC] and [WO] nebulae are quite similar to those of the "normal" PN. However, a slight difference can be noted, in that the [WO] tend to have higher Ne/O and S/Ar ratios, while among the [WC] both ratios are smaller. The *wels* also show a preference for having lower S/Ar ratios. Because this pattern is already present, if one considers only nebulae of the same excitation (e.g. 5), these differences appear to be real, and not to be artifacts caused by the use of ICF, for example.

There are two remarkable outliers, PNG 004.9 + 04.9 (one of the three nuclei of [WC 5-6] type) and PNG 011.9 + 04.2 (one of the four nuclei of type [WO 4p] which show very high velocity winds), which also stand out in diagrams of the other combinations of abundance ratios; neither object shows any obvious flaw in the observational material or analysis. In these objects, PSM01 had found unusually low Ne/O abundance ratios of 0.00343 and 0.00371, respectively. Our values (0.052 and 0.083) are higher, but still substantially lower than the solar value of 0.16. The other non-WR object in the vicinity is PNG 325.4 – 04.0 observed by Kingsburgh & Barlow (1994).

5. Other global relations

5.1. Diagnostic diagram

In the diagnostic diagram of the intensity ratios Hα/[N II] and Hα/[S II] (Fig. 13, after Cantó 1981 and Corradi et al. 1997), the nebulae of our sample cover the region occupied by planetary nebulae. Except for some preference of the [WO] objects to do not extend to high Hα/[S II] and Hα/[N II] ratios, no specific region for [WR] nebulae can be distinguished.

5.2. Dereddened flux and angular diameter

The diagram of dereddened Hβ flux and angular diameter allows some inferences on the number of ionizing photons from the central star: in an ionization bounded Strömgren sphere of radius R, the dereddened Hβ flux at a distance d depends on the number of ionizing photons as

$$\mathcal{N}_{\rm LyC} = \frac{4\pi}{3}\alpha_B R^3 n^2 = \frac{\alpha_B}{\alpha_{\rm eff}} \cdot 4\pi d^2 \cdot F_0({\rm H}\beta) \qquad (3)$$

with the coefficients α_B for all recombinations to excited levels and $\alpha_{\rm eff}$ for leading to the emission of Hβ photons. Using the relation $R/d = \sin(D) = D$ between angular diameter D and R, one obtains

$$F_0 d^2 \propto F_0/D^2 \cdot \mathcal{N}_{\rm LyC}^{2/3} \cdot n^{-4/3} \qquad (4)$$

and demanding that the ionized mass $M_{\rm ion} = 4\pi nmR^3/3$ remains constant, one gets

$$F_0 \propto D^2 \cdot \mathcal{N}_{\rm LyC}^{5/3} \cdot M_{\rm ion}^{-4/3} \qquad (5)$$

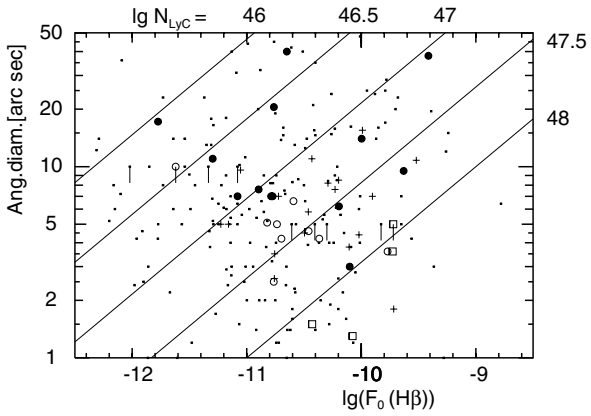

Fig. 14. Dereddened Hβ fluxes and angular diameters of nebulae with central stars of the various types: [WO] (filled circles), [WC] 5–6 and 4 (open circles), [WC] 10, 9, and 7–8 (open squares), *wels* (plus-signs), and any other (small dots). Short vertical lines mark objects whose diameter is only an upper limit. The lines of constant number of ionizing photons (in photons s^{-1}) are computed for ionization bounded nebulae of 0.25 solar masses.

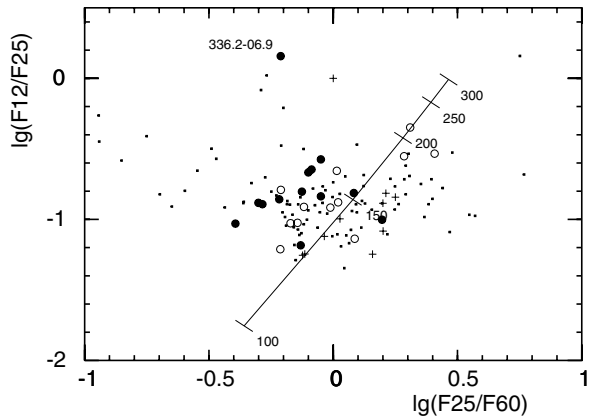

Fig. 15. Two-colour diagram of IRAS fluxes at 12, 25, and 60 μm. Symbols have the same meaning as in Fig. 8. Only high quality data is included. The line with ticks indicates the colours of black-body spectra between 100 and 300 K.

From the catalog of Acker et al. (1992) we take the optical diameter or – if that datum is uncertain, an upper limit, or the object is described as "stellar" – the radio diameter. Figure 14 shows that "normal" PN have a wide distribution in both diameter and number of ionizing photons. The same characteristic is also found among the [WO] types, as far as one can judge from the limited number of objects. However, the [WC] nebulae have a strong tendency to be smaller: except PNG 004.8 – 22.7 for which the optical diameter of 10 arcsec is only an upper limit, all nebulae are smaller than 6.6 arcsec (PNG 000.4 – 01.9). Late-type [WC] 10, 9, and 7–8 objects (shown as open squares) are smaller than about 5 arcsec, have high Hβ fluxes, and high number of ionizing photons, about $\lg \mathcal{N}_{\rm LyC} > 48$. All this ties in well with the notion that [WC] objects are young and compact nebulae. The *wels* have a fairly wide range in diameters and in ionizing photon number, although one may note that none is present with diameters larger than about 15 arcsec and $\lg \mathcal{N}_{\rm LyC} < 47.3$. One also has to keep in mind that these numbers depend on the ionized mass of the nebula, which might vary among the types.

5.3. Infrared colours

Planetary nebulae are strong infrared emitters, due to their heated dust: as the nebula expands, the dust cools and the dust colours redden. Fig. 15 shows the two-colour diagram for our samples. The [WR] objects are found mainly towards the left in the diagram and the *wels* are shifted to bluer colours, below the cooling line.

By using the dust model of Siebenmorgen et al. (1994), the IRAS fluxes can be calculated at any time following the nebular expansion, both for carbon-rich and oxygen-rich dust (see Acker et al. 1996a, and Gesicki et al. 2006). From the Fig. 15 of this paper and the Fig. 7 of Gesicki et al. (2006), the [WR] stars are displayed along evolutionary progression of carbon-rich nebular dust, from cool stars with bluer IRAS colours (like those of post-AGB stars) to hot stars with redder IRAS colours. But the *wels* sample appears to be shifted below the oxygen rich track. Note that most of the *wels* were classified as O-rich stars by Méndez (1991).

On the other hand, Gesicki et al. (2006) show that about 65% of the CSPNe have good IRAS detections, with different detection rates: respectively 52%, 53%, and 88% for "normal", *wels* and [WR] PNe, the latest being on average much stronger IRAS emitters. If one considers 25 and 60 μm only, the detection rates become 89%, 86% and 100%, i.e. the difference is rather reduced, which indicates that [WR] PNe (essentially [WC] PNe) are stronger emitter at 12 μm. This is indicative of small dust grains, which is not found in *wels*.

The [WR] evolution seems marked by the presence of nebular turbulence, almost universal for [WR] PNe, common for *wels* but rare for "normal" PNe (91%, 24%, and 7%, respectively), a difference which shows that the "normal" PNe are not closely related to the [WR] stars, as the different dynamics of the nebulae takes time to build up (Acker et al. 2002; Acker & Neiner 2003; Gesicki et al. 2006). Given the differences in IRAS colours, chemistry and carbon surface abundances of the [WC] stars, a sequence can be considered where they evolve too slowly to reach [WO] types while still surrounded by a bright nebula. Gesicki et al. (2006) show that strong correlation appears between enhanced 12 μm flux and turbulence for the [WC] PNe, leading to the formation of small grains. But this is not the case for the *wels* which show almost identical colours regardless of turbulence. The expansion is a strong function of metallicity, therefore the expansion of the nebulae around O-rich stars grows slower than around C-rich stars (Acker et al. 1996a), and shows lower dust abundance in the AGB wind (Wood et al. 1992). The very blue [WO 4] nebula PC 14 (PNG 336.2 – 06.9) is perhaps more compact than other [WO 4] PNe, with a lower expansion related to a lower metallicity. We also note that many [WC] stars show a unique feature in their nebular chemistry, with both PAHs and oxygen-rich dust and gas being present (Zijlstra 2001). This mixed chemistry is not seen among either [WR] PNe or any other group of PNe.

All these aspects confirm the analysis by Tylenda et al. (1993) who argue that the [WR] and the *wels* form two distinct groups: *wels* show very weak emission lines, and a different chemistry in the line forming wind, the N/C ratio being higher in *wels* than in [WC] (Acker et al. 1996a). The [WR] PNe seem to be more compact than the nebulae around *wels*, which indicates a different mass-loss history. The progenitor properties (age, metallicity, stellar activity) may play the major rôle in the formation of a *wels* or a [WC] star.

From the DENIS database at CDS we extracted the infrared colours for our objects (10 [WO], 14 [WC], 13 *wels*, and 94

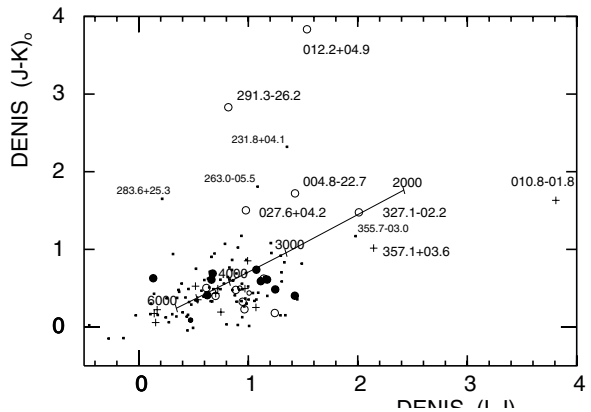

Fig. 16. The two-colour diagram of $I - J$ vs. $J - K$ from DENIS data. The line with ticks indicates colours from blackbody with temperatures from 3000 to 6000 K. The symbols are as in Fig. 8.

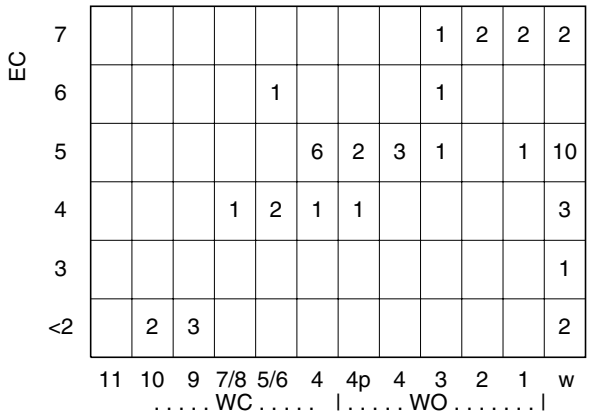

Fig. 17. Distribution of nebulae among central star spectral types and excitation class of the nebula. The column marked "w" refers to *wels* objects.

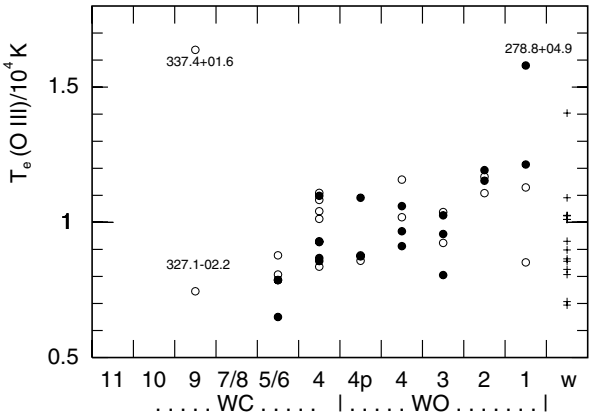

Fig. 18. Relation between spectral types and electron temperature from [O III] (filled circles) and from [N II] (open circles). *wels* are marked by a cross.

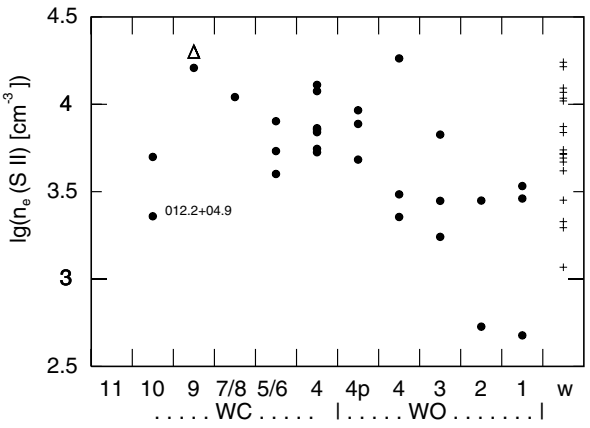

Fig. 19. Relation between spectral types and electron density from [S II]. "Δ" are the limit of density determination (marked 20.00H in Table 2). *wels* are marked by a cross.

non-WR nebulae). In the two colour diagram (Fig. 16) of the I(0.82 μm), J(1.25 μm) and K(2.15 μm) bands, most nebulae of all types cluster near colour temperatures of 4000 K. While none of the [WO] objects is found elsewhere, several [WC] nebulae are found at high $(J-K)_0$ colour indices: foremost PNG 012.2 + 04.9 and PNG 291.3 − 26.2 which have been suspected for the presence of hot dust (Górny et al. 2001), and also PNG 004.8 − 22.7, PNG 027.6 + 04.2, and PNG 327.1 − 02.2.

Likewise, two *wels* are found with high $(I - J)_0$ values: PNG 010.8 − 01.8 and PNG 357.1 + 03.6. Inspection of the DENIS data reveals that none of these objects has magnitude errors in excess of the other objects. Neither do we find correlations with other nebular properties, such as Hβ flux, extinction, or angular diameter.

6. Relations between central star and nebula

To explore the possibility of an evolutionary sequence from [WC 11] to [WO 1], we investigate the nebular properties as a function of the spectral type of their central stars. Since the excitation class is a measure of the temperature of the ionizing source, it is expected to be linked to the temperature of the central star. Figure 17 indicates a clear relation between spectral type and excitation class, in the sense that [WC] central stars are found in low excitation nebulae, while the early [WO] stars are surrounded by nebulae of highest excitation. The *wels* central stars are found in objects of any level of excitation. Given the small sample, we regard the large number with EC = 5 as an observational selection effect.

This is also evident in the electron temperatures, depicted in Fig. 18. Unfortunately, there are no measurements of the [O III] temperature in the low excitation nebulae, and the few reliable [N II] temperatures do not allow to follow this correlation among these types of objects.

Figure 19 shows that the electron density decreases along the sequence from cooler [WC 10] to hot [WO 1]. This ties in well with the notion of an evolutionary sequence: as the density decreases due to the nebular expansion, the central star becomes hotter. In contrast, the *wels* objects display a wide range of densities, and cannot be incorporated into this sequence.

All these results support an evolutionary sequence from [WC 11] central stars which are cool and surrounded by dense, low excitation nebulae towards hot [WO 1] stars with low density, high excitation nebulae.

The *wels* objects evidently belong to a different class of planetaries which do not appear to be evolutionarily related to the [WR] type nebulae.

7. Conclusions

Nebular spectra of 48 PN around central stars of [WR] and *wels* spectral type are analyzed for plasma properties and chemical compositions. Comparison of the results for [WC], [WO] and *wels* objects with the properties of "normal" non-WR type objects confirm that the nebulae of either group are very similar:

- they remain indistinguishable in Canto's diagnostic diagram;
- the relation of electron temperatures from [N II] and [O III] lines show the same trend and range;
- the average [O III] temperature in [WR] PN and *wels* objects is about 3000 K lower than in non-WR nebulae;
- they have the same average helium abundances, and abundance distributions. *wels* have slightly lower helium abundances;
- the nitrogen abundances in [WC] and [WO] nebulae are somewhat enhanced with respect to the Sun, while *wels* and non-WR PN have solar values;
- the N/O abundance ratio in both [WC] and [WO] PN is about thrice solar, somewhat higher than in non-WR (less than twice solar). But *wels* objects have a much lower ratio, of nearly solar value;
- O, Ne, S, Ar abundances are nearly solar in all groups;
- [WC] and *wels* nebulae tend to be smaller than [WO] and non-WR objects;
- the number of ionizing photons covers the same range and has the same average value;
- in the IRAS two-colour diagram, *wels* are shifted to bluer colours than the other [WR] PN;
- in the DENIS two-colour diagram some [WC]s are found at high $(J-K)_0$ values while two *wels* have high $(I-J)_0$ colour indices.

With respect to the central star's spectral type, some clear trends are present: From [WC 11] to [WO 1],

- the excitation class rises, hence the temperature of the star's ionizing spectrum;
- the electron temperature rises;
- the electron density decreases.

As one would expect for an evolutionary sequence from late to early spectra type, as the star heats up and the nebula expands. The *wels* nebulae have properties that cover a wide range, and they evidently belong to a separate subclass of PN, and do not appear to be evolutionarily related to the [WR] type nebulae.

Thus our results corroborate the evolutionary sequence from [WC 11] central stars which are cool and surrounded by dense, low excitation nebulae towards hot [WO 1] stars with low density, high excitation nebulae with embedded cooler dust. On the other hand, there is no evidence for the *wels* being linked by evolution to the [WR] PN. Rather they seem to constitute a separate class of objects with a variety of nebular properties. Their lower N/O ratio and the hint of a lower He/H abundance suggests that they might have formed from less massive progenitor stars than the other PN.

Acknowledgements. We thank Sophie Durand for a first measurement of the majority of the spectra. We wish to express our thanks to the referee for detailed comments and constructive suggestions.

References

Acker, A., Neiner, C. 2003, A&A, 403, 659 (AN03)
Acker, A., Samland, M., Köppen, J., & Stenholm, B. 1989, ESO Messenger, 58, 44
Acker, A., Köppen, J., Stenholm, B., & Raytchev, B. 1991, A&AS, 89, 237
Acker, A., Ochsenbein, F., Stenholm, B., et al. 1992, Strasbourg-ESO Catalogue of Galactic Planetary Nebulae (SECGPN), ESO, Garching
Acker, A., Górny, S. K., & Cuisinier, F. 1996a, A&A, 305, 944
Acker, A., Marcout, J., & Ochsenbein, F. 1996b, First Supplement to the SECGPN, Observatoire de Strasbourg
Acker, A., Gesicki, K., Grosdidier, Y., & Durand, S., 2002, A&A, 384, 620
Aller, L. H. 1956, Gaseous Nebulae, The international Astrophysics Series, Vol. III, (London: Chapman & Hall)
Aller, L. H. 1984, Physics of Thermal Gaseous Nebulae, Reidel, Dordrecht
Aller, L. H., Keyes, C. D. 1980, Ap&SS, 72, 203 (AK80)
Aller, L. H., Czyzak, S. J. 1983, ApJ, 51, 211 (AC83)
Aller, L. H., Keyes, C. D. 1987, ApJS, 65, 405 (AK87)
Aller, L. H., Keyes, C. D., & Czyzak S. J. 1981, ApJ, 250, 596
Aller, L. H., Keyes, C. D., & Feibelman, W. 1986, ApJ, 311, 930 (AKF86)
Barker, T. 1978, ApJ, 219, 914
Berrington, K. A., Kingston, A. E. 1988, J. Phys. B, 20, 6331
Brocklehurst, M. 1972, MNRAS, 157, 211
Cantó, J. 1981, in Investigating the Universe, Reidel, Dordrecht, p. 95
Corradi, R. L. M., Villaver, E., Mampaso, A., & Perinotto, M. 1997, A&A, 324, 276
Crowther, P. A., De Marco, O., & Barlow, M. J. 1998, MNRAS, 296, 367 (CMB98)
Cuisinier, F., Acker, A., & Köppen, J. 1996, A&A, 307, 215 (CAK96)
Cuisinier, F., Maciel, W. J., Acker, A., Köppen, J., & Stenholm, B. 2000, A&A (CMAKS00)
DENIS database at `http://cdsweb.u-strasbg.fr/denis.html`
Gesicki, K., Zijlstra, A. A., Acker, A., Gorny, S. K., Gozdziewski, K., & Walsh, J. R. 2006, A&A, 451, 925
Górny, S. K., Stasińska, G. 1995, A&A, 303, 893
Górny, S. K., Tylenda, R. 2000, A&A, 362, 1008
Górny, S. K., Stasińska, G., Szczerba, R., & Tylenda, R. 2001, A&A, 377,1007
Górny, S. K., Stasińska, G., Escudero, A. V., & Costa, R. D. D. 2004, A&A, 427, 231
Kingsburgh, R. L., Barlow, M. J. 1994, MNRAS, 271, 257 (KB94)
Köppen, J., Acker, A., & Stenholm, B. 1991, A&A, 248, 197
Méndez, R. H. 1991, IAU Symp., 145, 375
Mendoza, C. 1983, IAU Symp., 103, 143
Peimbert, M., Torres-Peimbert, S. 1983, IAU Symp., 103 , 233
Peña, M., Stasińska, G., & Medina, S. 2001, A&A, 367, 983 (PSM01)
Samland, M., Köppen, J., Acker, A., & Stenholm, B. 1992, A&A, 264, 184
Siebenmorgen, R., Zijlstra, A. A., & Krgel, E. 1994, MNRAS, 271, 449
Shaw, A. R., Kaler, J. B. 1989, ApJS, 69, 495 (SK89)
Tylenda, R., Acker, A., Stenholm, B., & Köppen, J. 1992, A&AS, 95, 377 (TASK92)
Tylenda, R., Acker, A., & Stenholm, B. 1993, A&AS, 102, 595
Wood, P. R., Whiteoak, J. B., Hugues, S. M. G., et al. 1992, ApJ, 397, 552
Zijlstra, A. A. 2001, Ap&SS, 275, 79

Online Material

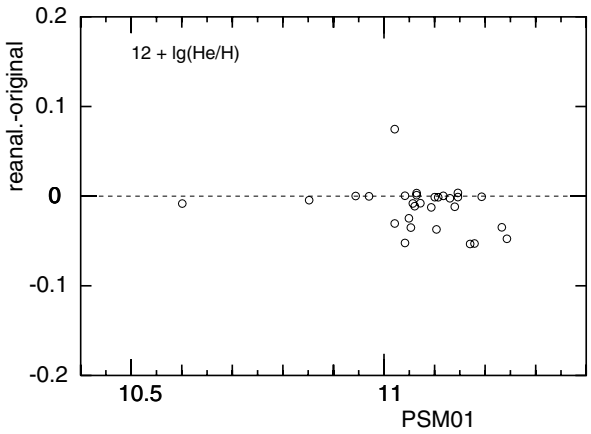

Fig. 20. The helium abundances of the PN observed by PSM01 compared to the values found by HOPPLA from the same data.

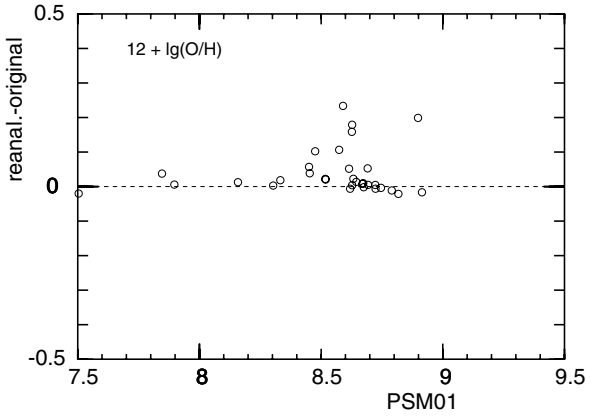

Fig. 21. The oxygen abundances of the PN observed by PSM01 compared to the values found by HOPPLA from the same data.

Appendix A: Comparison of the methods

We reanalyzed with HOPPLA the dereddened line intensities of the objects in the other works and compare the plasma parameters and abundances with the authors' original values (except for CAK96 and CMAKS00 who also use HOPPLA).

Since both HOPPLA and PSM01 use nearly the same atomic data, and use rather similar strategies, the reanalysis of their data gives almost identical results: both [O III] and [N II] electron temperatures are retrieved within 100 K (i.e. within the 3 decimal places of the authors' data), and the [S II] densities are within 0.05 dex. As shown in Fig. 20, the helium abundances mostly agree within 0.01 dex; however, for several high excitation objects (PNG 017.9 – 04.8, PNG 061.4 – 09.5, PNG 144.5 + 06.5, PNG 161.2 – 14.8, PNG 189.1 + 19.8, PNG 243.3 – 01.0, PNG 278.1 – 05.9, PNG 278.8 + 04.9, PNG 286.3 + 02.8) HOPPLA yields a smaller value, by as much as 0.06 dex. None of the objects shows discrepancies in electron density or temperature; however, in PNG 061.4 – 09.5 and PNG 278.1 – 05.9 the He I intensity is given as a single digit only (4 and 5), which could mean an uncertainty of as much as 20 percent. Another exception is PNG 356.2 – 04.4 for which a higher He abundance is found (by 0.08 dex). The origin for this discrepancy could not be found. The oxygen abundances (Fig. 21) are recovered within 0.1 dex, with the exceptions of PNG 061.4 – 09.5, PNG 161.2 – 14.8, PNG 189.1 + 19.8, PNG 243.3 – 01.0, PNG 278.8 + 04.9, and PNG 286.3 + 02.8 which have values

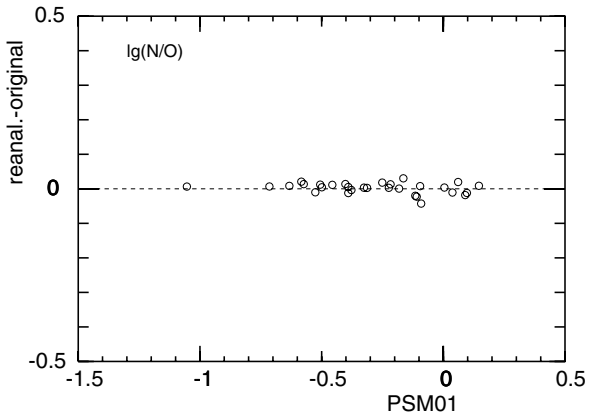

Fig. 22. The N/O abundance ratios of the PN observed by PSM01 compared to the values found by HOPPLA from the same data.

as much as 0.2 dex higher than in PSM01. The origin is that in these high excitation objects the oxygen ICF depends on the (high) He^{++}/He ratio which propagates and amplifies the deviation found in the He abundances. The maximum deviation in the N/O abundance ratio (Fig. 22) is 0.05 dex in PNG 004.9 + 04.9. We conclude that both methods give nearly identical results.

We refrain from showing for the other works the plots of comparing original and re-derived values for all quantities, but present the essential results in Table 5 in numerical form. We summarize the inspection of the plots of key quantities:

- KB94 include lines from the range 1200–3000 ÅẆhether or not these lines are included in the analysis, has rather little impact, but in all plots we show only the results based on the optical lines. The [O III] temperature is recovered within 300 K, with several outliers which cause a non-zero mean and a large dispersion. The [N II] temperature shows a substantially larger dispersion, but with all deviations being within 1000 K; the majority of the objects give higher temperatures, causing a substantial offset. Electron densities are recovered by 0.1 dex, with seven exceptions. Plasma parameters can be obtained from the published spectra for 53 objects. Helium abundances are within 0.05 dex; three objects have lower abundances and two give higher values. The oxygen abundances show a strong scatter up to 0.4 dex without significant offset. The deviations in the N/O ratio are as large as 0.5 dex, with a clear tendency for HOPPLA getting larger values.
- the data of AC83 and AK87 display a similar behaviour: the temperatures (composed from several diagnostic ratios) are within about 1000 K of the [O III] temperatures in the reanalysis, with 3 outliers. Electron densities show a strong scatter as well as a systematic offset when compared with our values from [S II], because the published values are based on averages from different diagnostic line ratios. The helium abundances are systematically lower (by about 0.05 dex) than in the reanalysis, with a scatter of the same magnitude. This offset is due to our inclusion of the corrections of the He I emissivities for collisional excitation based on Berrington & Kingston (1988). Oxygen abundances show significant scatter but without any offset. The N/O ratio has strong dispersion with little offset.

Often the reason for one object to show a strong deviation in the results can be traced to some particular cause, such as a diagnostic line ratio being at or close to the limit of its sensitivity,

Table 5. Results of the reanalysis of PN spectra from previous studies using the HOPPLA code. The averages and the dispersions are given for the differences of the original values and our results. Default values used by HOPPLA in the absence of diagnostic lines or in the high density limit are not taken into account. Note that the electron temperatures and densities given by AC83 and AK87 are the values adopted from combining different diagnostic line ratios. The number of objects in each sample refers to those with helium abundances. For KB94 we also show the results based on the optical lines only (3700 ... 8000 Å).

	AC83		AK87		KB94		KB94 (opt.)		PSM01	
No.objects	18		42		52		52		31	
	mean	disp.	mean	disp.	mean	disp.	mean	disp.	mean	disp.
T([OIII])	(−260)	(370)	(70)	(410)	−120	230	−180	220	20	60
T([NII])	—	—	—	—	−480	430	−580	320	10	100
lg(n[SII])	(0.073)	(0.155)	(−0.060)	(0.198)	−0.003	0.109	−0.003	0.109	0.005	0.022
He/H	0.039	0.024	0.037	0.033	0.010	0.028	0.004	0.025	0.011	0.024
N/H	−0.072	0.154	0.055	0.185	−0.157	0.210	−0.104	0.160	−0.043	0.072
O/H	0.004	0.212	0.033	0.145	−0.041	0.134	−0.009	0.115	−0.040	0.065
Ne/H	0.047	0.123	0.016	0.145	−0.055	0.146	−0.022	0.132	−0.047	0.061
S/H	0.063	0.162	−0.011	0.223	−0.067	0.184	−0.088	0.163	—	—
Ar/H	0.196	0.139	0.197	0.167	−0.116	0.199	0.119	0.198	—	—
N/O	−0.102	0.212	0.014	0.184	−0.120	0.187	−0.092	0.144	−0.002	0.015

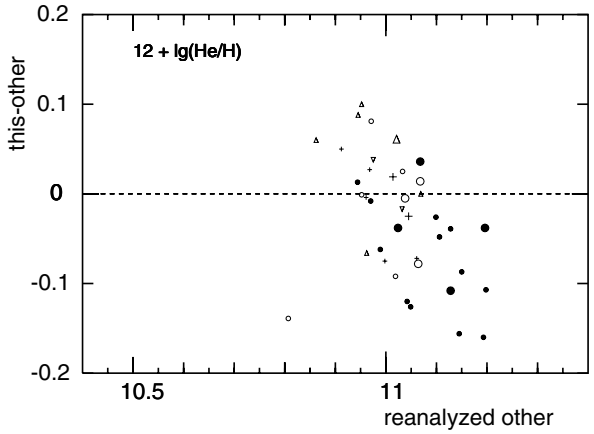

Fig. 23. Comparison of the helium abundances found in this work with the values obtained by reanalysis of the data from the other works. The symbols are the same as in Fig. 3; smaller symbols denote those objects which HOPPLA assumed default values for the electron temperatures or density.

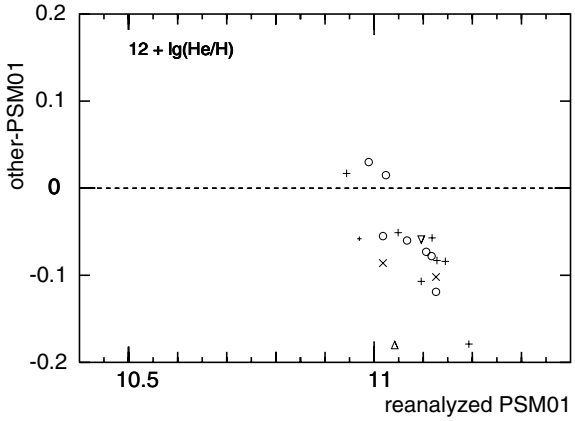

Fig. 24. Similar to Fig. 23, but comparing the reanalyzed PSM01 data with the reanalyzed data of AC83 (×), AK87, KB94, CAK96, and CMAKS00, using the same symbols as in Fig. 3.

resulting in a propagation of this error to other quantities. It would go beyond the aims of this paper to discuss these objects in detail, and thus trace in even more detail the origins of the differences found.

Appendix B: Comparison of the observational data

For the objects that we have in common with other works, we compare the results from the reanalysis with HOPPLA of their spectra with the present work. This reflects the differences in the measured intensities.

In Fig. 23 we compare our He/H abundances with the other studies. One notes a rather clear trend that we get lower helium abundances from our own data than from the the data of PSM01, especially for higher abundances. The results from the other data also are in line with this trend, although the fewer numbers do not allow to make a firm conclusion. As shown in Fig. 4, such a trend is already present in the intensities of the He I 5876 Å line.

However, if one compares the reanalyzed data of PSM01 with the other works, another clear correlation is found, as depicted in Fig. 23. Again, this is reflected in PSM01 getting higher He I intensities for the stronger lines than by previous studies (Fig. 25).

With the other elements, no such clear trend is found, partially because the scatter is substantially larger. We summarize the results as average and dispersion of the deviations found: Table 6 gives the comparison between our data and the reanalysis of the PSM01 data. The plasma parameters do not show a systematic offset, except for the [N II] temperatures, but a large scatter, which indicates differences in S/N ratio which affect the faint lines. The argon abundances obtained from the spectra of PSM01 are substantially lower than from our spectra, because in PSM01 the intensity for the [Ar III] 7135 Å line - the dominant stage of ionization - are given only for three objects.

In the abundances of N/H, O/H, Ne/H, and S/H there exist also offsets that are marginally acceptable, and one notes rather appreciable scatter. As the lower offsets and dispersions in the Ne/O and S/O ratios indicate, the scatter originates from the O/H determinations and is translated to the other elements by applying the ICFs. The scatter in O/H comes from the electron temperature differences, and principally from differences in the intensity of the [O III] 4363 Å line. As already seen in Fig. 7, the scatter in the [O III] electron temperatures is much larger than the differences due to the analysis methods. If we compare

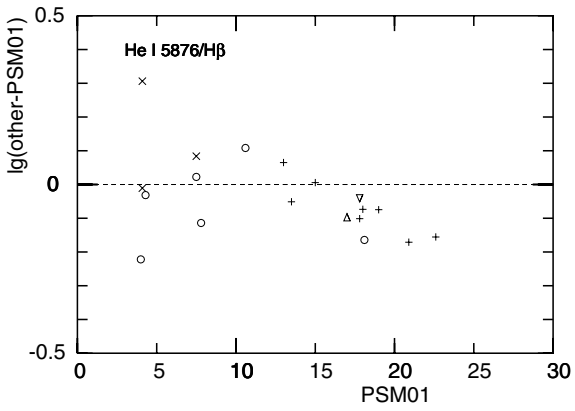

Fig. 25. Similar to Fig. 4, but comparing the PSM01 data with the data of AC83, AK87, KB94, CAK96, and CMAKS00, using the same symbols as in Fig. 24.

Table 6. The means and dispersions of the differences between the reanalyzed PSM01 data and this work, along with the formal error bars. For the abundances we use only values for which HOPPLA does not mark as uncertain, such as indicated by colons in Table 3 (on-line version). For the line intensities, the differences of $\lg(I/I(\mathrm{H}\beta))$ are used. The last column gives the number of objects.

	mean	disp.	No.
T([OIII])	−10 ± 290	1130 ± 210	15
T([NII])	840 ± 330	1100 ± 240	11
lg(n[SII])	−0.142 ± 0.109	0.464 ± 0.077	18
lg(He/H)	0.053 ± 0.019	0.078 ± 0.013	17
lg(N/H)	0.121 ± 0.065	0.242 ± 0.046	14
lg(O/H)	−0.001 ± 0.043	0.161 ± 0.031	14
lg(Ne/H)	−0.123 ± 0.059	0.212 ± 0.042	13
lg(S/H)	0.112 ± 0.078	0.270 ± 0.055	12
lg(Ar/H)	0.128 ± 0.068	0.096 ± 0.048	2
lg(N/O)	0.122 ± 0.054	0.203 ± 0.038	14
lg(Ne/O)	0.055 ± 0.020	0.073 ± 0.014	13
lg(S/O)	−0.025 ± 0.020	0.070 ± 0.014	12
[O III] 5007	0.026 ± 0.019	0.080 ± 0.014	17
He II 4686	−0.091 ± 0.082	0.218 ± 0.058	7
He I 5876	0.056 ± 0.015	0.064 ± 0.011	17
[O III] 4363	−0.009 ± 0.056	0.201 ± 0.039	13
[S II] 6725	0.047 ± 0.037	0.154 ± 0.026	17

the reanalysed PSM01 data with earlier data of the same objects, we find similar results; however, the discrepances in the line intensities are stronger, as can be seen from Fig. 25.

Let us consider this more closely in Fig. 26: we compare the differences between our values and PSM01 for the [O III] 4363 Å intensities and the derived oxygen abundances. While for the majority of objects these differences are less than 0.1 dex, outliers like PNG 006.8 + 04.1 and PNG 002.2 + 09.4 exhibit [O III] intensities that differ by as much as a factor of 2, and their abundances differ correspondingly, as indicated by the diagonal line. PNG 006.8 + 04.1 is one of the fainter objects of the sample which may thus be subject to a lower signal-to-noise ratio. PNG 002.2 + 09.4 is one of the brighter ones, in whose spectrum no fault or anomality was noticed.

The deviation of PNG 011.9 + 04.2 has yet a different origin: the density sensitive [S II] line ratio is close to its high density limit. Thus the slightly lower intensity ratio measured in our spectra of $I(6717)/I(6731) = 0.50$ (PSM01: 0.53) gives a

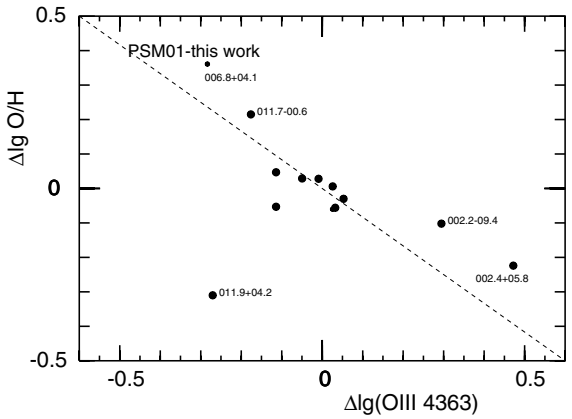

Fig. 26. The correlation between the deviations of oxygen abundances and intensities of the [O III] 4363 Å line for the nebulae in common with PSM01. The diagonal line indicates a linear relation between the two deviations.

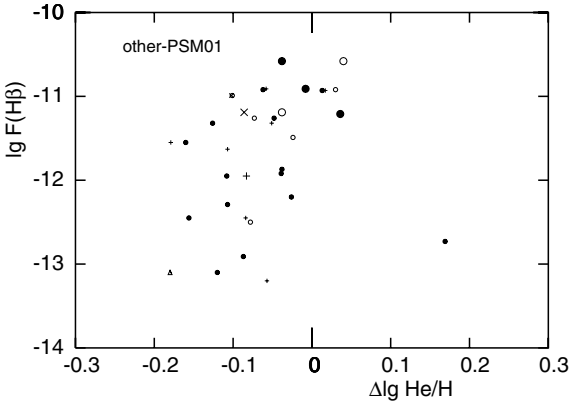

Fig. 27. Relation of the difference between helium abundances from the reanalyses of the data of AC83 (×), AK87(+), KB94(○), CAKS96 (△), and this work (•) with those from PSM01. Smaller symbols indicate nebulae where default values for electron temperature or density had to be assumed by HOPPLA.

significantly higher density of 9245 cm^{-3} (2562). Due to the effects of collisional deexcitation the nearly identical 5755 Å line intensities 6.58 (7.10) give a significantly [N II] temperature 8576 K (9670 K), and hence higher O^+/H^+ ionic abundance 3.167×10^{-4} (1.030×10^{-4}). This is more important than the change in [O III] temperature 10907 K (9965 K) from the larger [O III] 4363 Å intensity of 4.1 (2.2)!

In the quest to identify the origin of the deviation of the helium abundances derived by us and PSM01, the only clear trend is found to exist between this deviation and the absolute Hβ flux, as presented in Fig. 27. We note that the results from the other works are in line with the results of this work, in that large negative differences are found in faint objects. Because of the larger number of objects in common, this trend is more evident with our data.

Comparing the differences in the intensities of the He I 5876 Å line from the corresponding works (Fig. 28), one notes that for fainter nebulae the intensities from PSM01 tend to be smaller than in the other works, including our own. Inspection of the [S II] 6725 Å and [O III] 4363 Å lines, which are of comparable intensity, does not reveal a trend as clear as seen in the He I line.

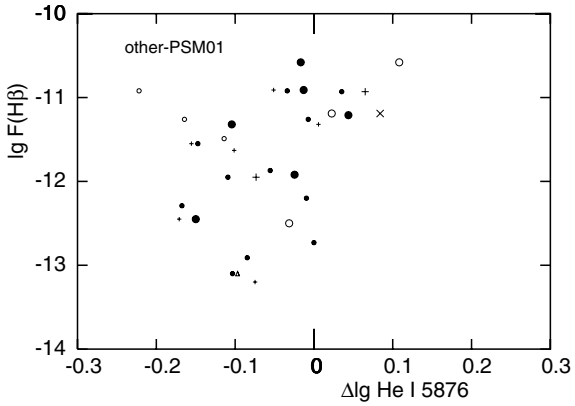

Fig. 28. Similar to Fig. 27, but for the intensity of the He I 5876 Å line.

We conclude that there exists a small but systematic difference in the helium abundances between our work and PSM01, in that the nebular He I lines in fainter objects have been either underestimated by us (and the other works) or overestimated by PSM01. Since the observational conditions are quite similar, yielding spectra of the same signal-to-noise ratio, we cannot determine the reason with certainty. Because a thorough reanalysis of our data did not reveal a possible underestimation of He I 5876 Å fluxes, and the values are found to be in good agreement with the other He I lines, we tend to prefer our results.

This difference is larger than the differences due to the analysis methods and larger than uncertainties in atomic data, and thus it is somewhat annoying; however, it is not large enough to affect the findings on the status of WRPN.

Table 3. Elemental abundances for the nebulae. Uncertain values are marked with a colon. Q and EC are the same as in Table 2.

PN G	common name	Spec.Type	Q	EC	He	N	O	Ne	S	Ar	Cl
000.4 – 01.9	M 2-20	WC5-6	A	4	11.06 :	8.17	8.78	7.85	7.23	6.61 :	5.21 :
002.2 – 09.4	Cn 1-5	WO4pe	A	5	11.10	8.52	8.76	8.24	7.22	6.68	5.27 :
002.4 + 05.8	NGC 6369	WO3	A	5	10.92 :	8.29	8.91	8.40	7.04	6.37 :	—
003.1 + 02.9	Hb 4	WO3	A	6	11.02	8.60	8.72	8.16	7.08	6.49	5.17 :
004.8 – 22.7	He 2-436	WC4	C	5	11.07 :	7.29 :	8.50 :	7.75 :	6.74 :	5.86 :	4.28 :
004.9 + 04.9	M 1-25	WC4	A	4	11.09 :	8.41	8.75	7.47	7.26	6.66	5.31 :
006.0 – 03.6	M 2-31	WC4	A	5	11.02	8.49	8.70	8.06	7.04	6.40	4.97 :
006.4 + 02.0	M 1-31	wels	A	5	11.09 :	8.31	8.49	—	6.87	6.42 :	5.05
006.8 + 04.1	M 3-15	WC4	A	5	10.99 :	8.01	8.36	7.68	6.72	6.14 :	4.77 :
009.4 – 05.0	NGC 6629	wels	A	5	10.96	7.56	8.67	7.96	6.45	6.23 :	5.84
010.8 – 01.8	NGC 6578	wels	A	5	11.03	7.94	8.75	8.17	6.88	6.83	5.20
011.7 – 00.6	NGC 6567	wels	A	5	10.96	7.61	8.42	7.67	6.41	5.73	4.70
011.9 + 04.2	M 1-32	WO4pe	A	4	11.07 :	8.35	8.66	7.58	7.34	6.89	4.93 :
012.2 + 04.9	PM 1-188	WC10	C	<2	—	8.12 :	8.57 :	—	6.99 :	5.84 :	—
016.4 – 01.9	M 1-46	wels	A	<2	10.88	7.95	8.87	—	7.13	6.53 :	5.24 :
017.9 – 04.8	M 3-30	WO1	C	7	11.09 :	7.02 :	8.48 :	—	6.91 :	6.53 :	—
019.4 – 05.3	M 1-61	wels	A	5	10.90	8.06	8.49	7.87	6.58	6.17	5.48 :
019.7 – 04.5	M 1-60	WC4	A	5	11.07	8.96	8.78	8.22	7.21	6.67	4.72 :
020.9 – 01.1	M 1-51	WO4pe	A	5	11.08 :	8.29	8.92	8.52	7.28	6.54 :	5.24 :
027.6 + 04.2	M 2-43	WC7-8	C	4	10.92 :	7.24 :	8.63 :	7.10 :	6.87 :	6.16 :	4.55 :
029.2 – 05.9	NGC 6751	WO4	A	5	11.06 :	8.34	8.69	8.06	6.94	6.46 :	—
034.6 + 11.8	NGC 6572	wels	A	5	11.04	8.31	8.60	7.93	6.52	6.33	4.83
038.2 + 12.0	Cn 3-1	wels	A	<2	10.68	7.95	8.79	—	6.99	6.15	4.95 :
048.7 + 01.9	He 2-429	WC4	A	4	11.06 :	8.41	8.77	—	7.24	6.81	5.34 :
055.5 – 00.5	M 1-71	wels	A	5	11.03 :	8.62	8.76	8.01	6.52	6.50	4.93
057.2 – 08.9	NGC 6879	wels	A	5	10.99	7.93	8.52	7.87	6.80	6.14	4.64 :
061.4 – 09.5	NGC 6905	WO2	B	7	10.93 :	8.47	8.85	8.18	7.13	6.18	5.60 :
068.3 – 02.7	He 2-459	WC9	C	<2	9.48 :	7.77 :	7.85 :	—	7.03 :	—	4.45 :
253.9 + 05.7	M 3-6	wels	A	5	11.05	7.77	8.71	8.15	6.73	6.35	5.07 :
258.1 – 00.3	He 2-9	wels	A	4	10.96 :	7.73	8.44	7.69	6.57	6.80	4.70 :
274.6 + 02.1	He 2-35	wels	A	5	11.00	7.23	8.73	8.10	6.77	6.24	4.95 :
278.1 – 05.9	NGC 2867	WO2	A	7	10.99	7.99	8.64	7.96	6.71	6.04	4.97 :
278.8 + 04.9	PB 6	WO1	A	7	11.16	8.94	8.79	8.23	6.82	6.12	—
285.4 + 01.5	Pe 1-1	WO4	A	5	10.99 :	8.15	8.62	8.02	6.62	6.34	4.91
291.3 – 26.2	Vo 1	WC10	C	<2	11.02 :	7.39 :	8.65 :	—	6.58 :	—	—
292.4 + 04.1	PB 8	WC5-6	A	6	11.08	8.33	8.82	8.18	6.84	6.69	5.36
300.7 – 02.0	He 2-86	WC4	A	5	11.05 :	8.79	8.67	7.93	7.13	6.54	5.13 :
307.2 – 03.4	NGC 5189	WO1	A	5	10.72 :	8.41	8.38	7.75	7.53	6.41	4.85 :
327.1 – 02.2	He 2-142	WC9	B	<2	10.67 :	8.22 :	8.95 :	—	6.90 :	5.40 :	5.12 :
331.3 + 16.8	NGC 5873	wels	A	7	10.95	7.22	8.38	7.74	7.23 :	5.67 :	5.18
336.2 – 06.9	PC 14	WO4	A	5	11.03	8.25	8.77	8.12	7.06	6.38	5.09 :
337.4 + 01.6	Pe 1-7	WC9	B	<2	10.17 :	7.22 :	6.93 :	—	6.10 :	4.97 :	3.82 :
351.1 + 04.8	M 1-19	wels	A	4	11.01 :	8.39	8.86	8.17	7.06	6.62 :	5.28 :
355.2 – 02.5	H 1-29	WC4	A	5	11.01 :	8.26	8.67	8.04	6.81	6.29	4.95 :
355.9 – 04.2	M 1-30	wels	A	3	11.09	8.49	8.79	7.89	7.30	6.76	5.28 :
356.7 – 04.8	H 1-41	wels	A	7	11.03	8.00	8.57	7.87	6.78	6.09	5.27
357.1 + 03.6	M 3-7	wels	A	4	11.00	7.91	8.68	7.98	7.06	6.36 :	5.11 :
358.3 – 21.6	IC 1297	WO3	A	7	11.05	8.37	8.77	8.10	7.10	6.27	5.37